Freestanding Laser-Induced Graphene/Carbon Fiber Frameworks Functionalized with NiO for High-Performance Non-Enzymatic Glucose Sensing

Guangmeng Chen [1], *Ziqiang Hu* [1], *Yuan Liu* [2], *Li Jia* [1], *Weiwei Zhao* [1], *Xiaoqing Liu** [1]

[1] State Key Laboratory of Advanced Marine Materials, Ningbo Institute of Materials Technology and Engineering, Chinese Academy of Sciences, Ningbo, Zhejiang 315201, China

[2] College of Chemistry and Chemical Engineering, Tarim University, Alar 843300, P. R. China

Corresponding authors:

Xiaoqing Liu, E-mail address: liuxq@nimte.ac.cn

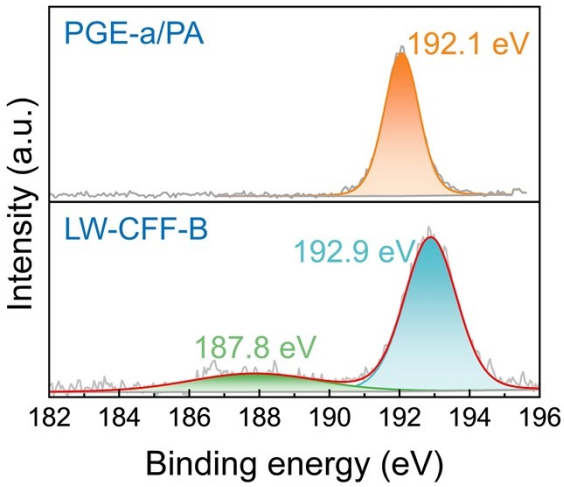

Figure S1. High-resolution XPS spectrum of B 1s for PGE-a/PA and LW-CFF-B.

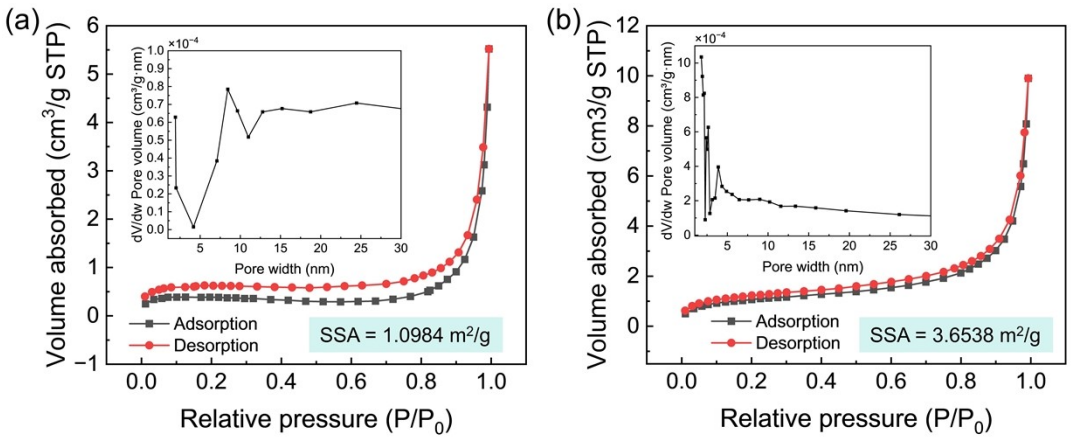

Figure S2. N_2 adsorption-desorption isotherms of (a) LW-CFF (inset: related pore size distribution plot), (b) LW-CFF-B (inset: related pore size distribution plot).

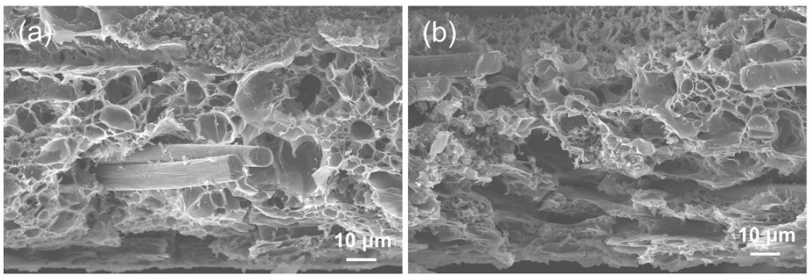

Figure S3. SEM cross-sectional images of LW-CFF-B (a) and LW-CFF-B-Ni (b).

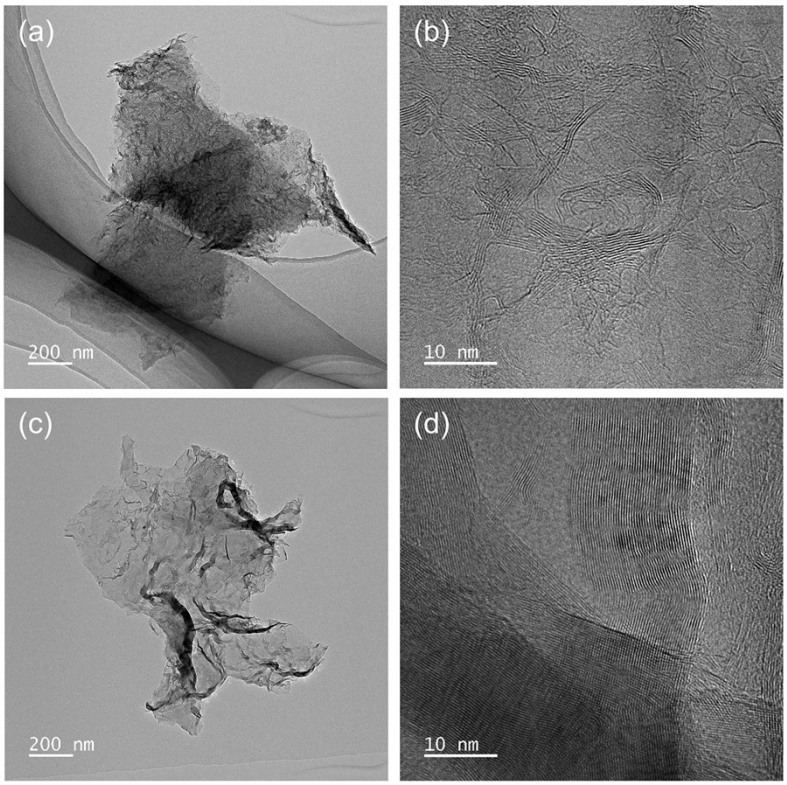

Figure S4. TEM and HR-TEM images of LW-CFF (a-b) and LW-CFF-B (c-d).

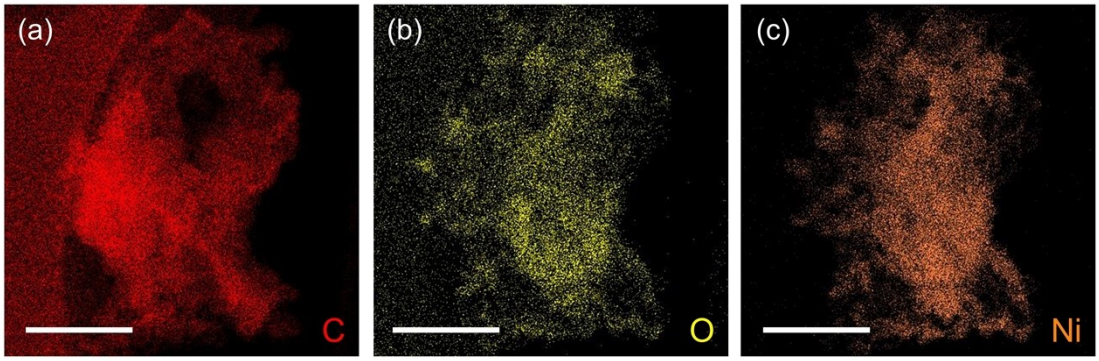

Figure S5. Elemental mapping of LW-CFF-B-Ni taken via STEM mode, the scale bar is 500 nm.

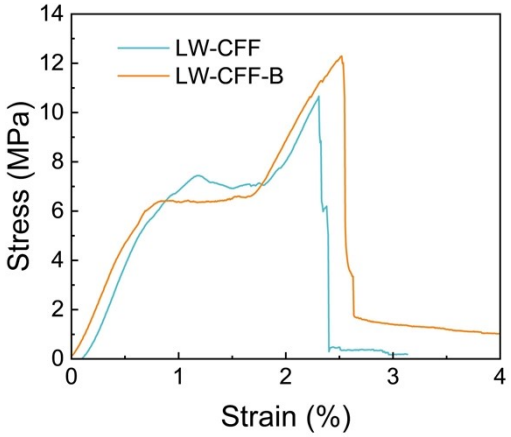

Figure S6. Stress-Strain curves of LW-CFF and LW-CFF-B.

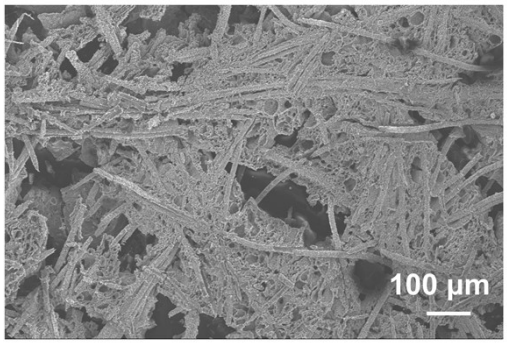

Figure S7. SEM image of LW-CFF-B film with PA content of 30 wt.%.

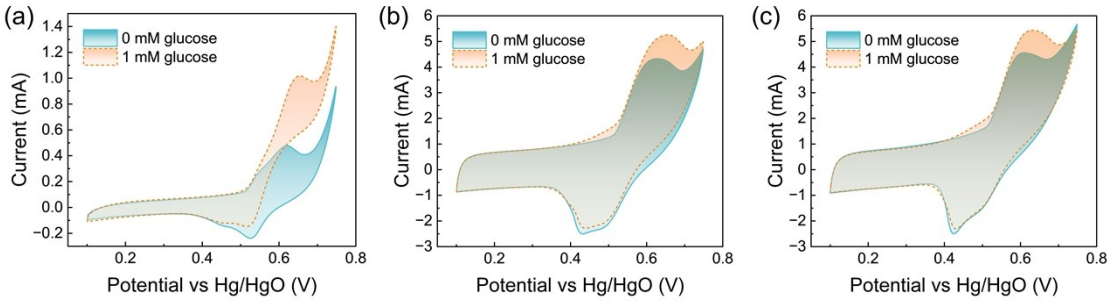

Figure S8. CV curves of LW-CFF-Ni with second laser power of 1.5 W (a), 3.5 W (b) and 4.5 W (c).

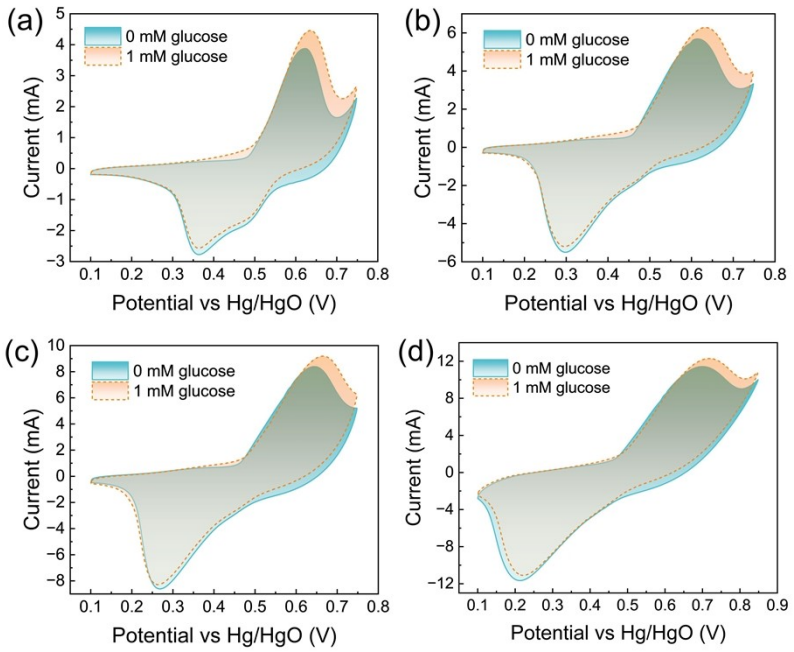

Figure S9. CV curves of LW-CFF-Ni with $Ni(NO_3)_2$ concentration of 0.05 M (a), 0.1 M (b), 0.2 M (c) and 0.4 M (d).

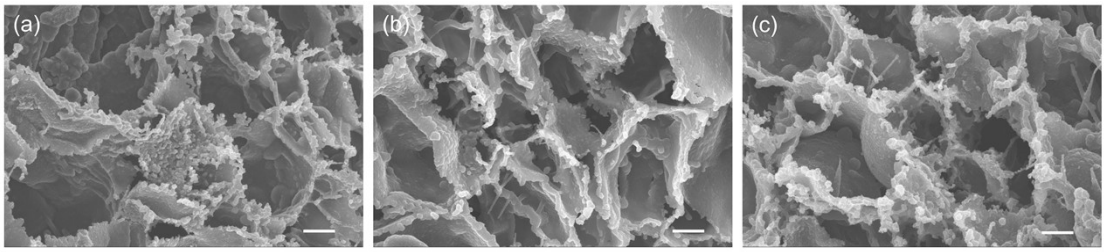

Figure S10. SEM images of LW-CFF-B-Ni with $Ni(NO_3)_2 \cdot 6H_2O$ concentration of 0.05 M (a), 0.1 M (b), and 0.2 M (c), the scale bar is 2 μm.

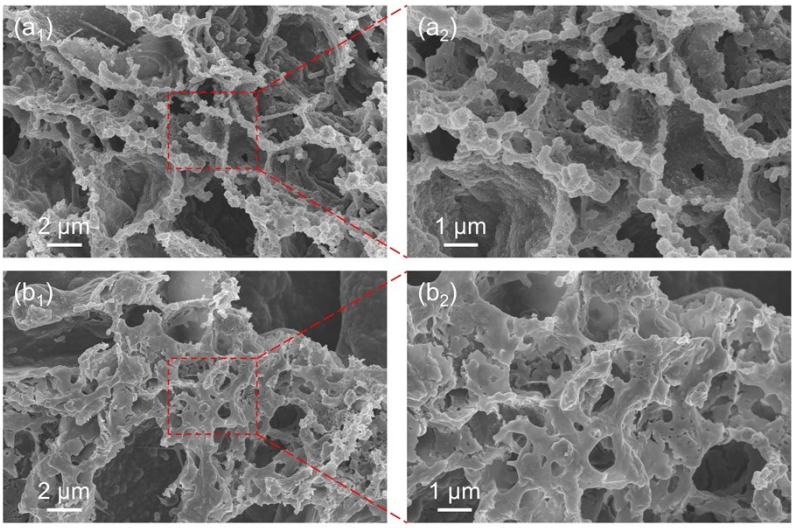

Figure S11. Detailed SEM images of LW-CFF-B-Ni with $Ni(NO_3)_2 \cdot 6H_2O$ concentration of 0.3 M (a) and 0.4 M (b).

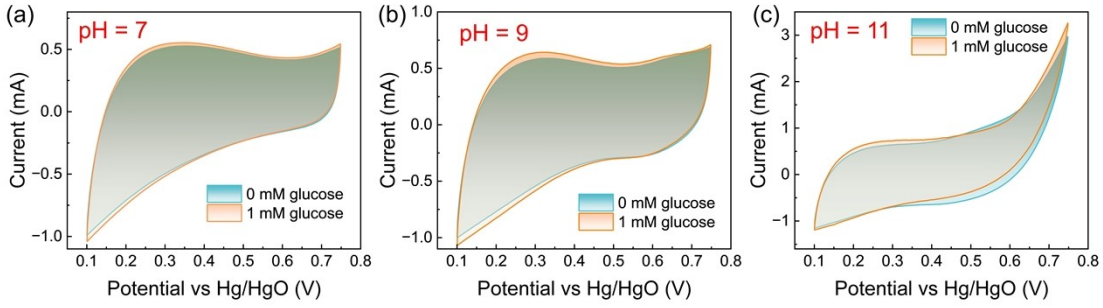

Figure S12. CV of LW-CFF-B-Ni electrode recorded in the absence and presence of 1 mM glucose in Neutral and weakly alkaline buffer solutions: (a) pH = 7, (b) pH = 9, (c) pH = 11.

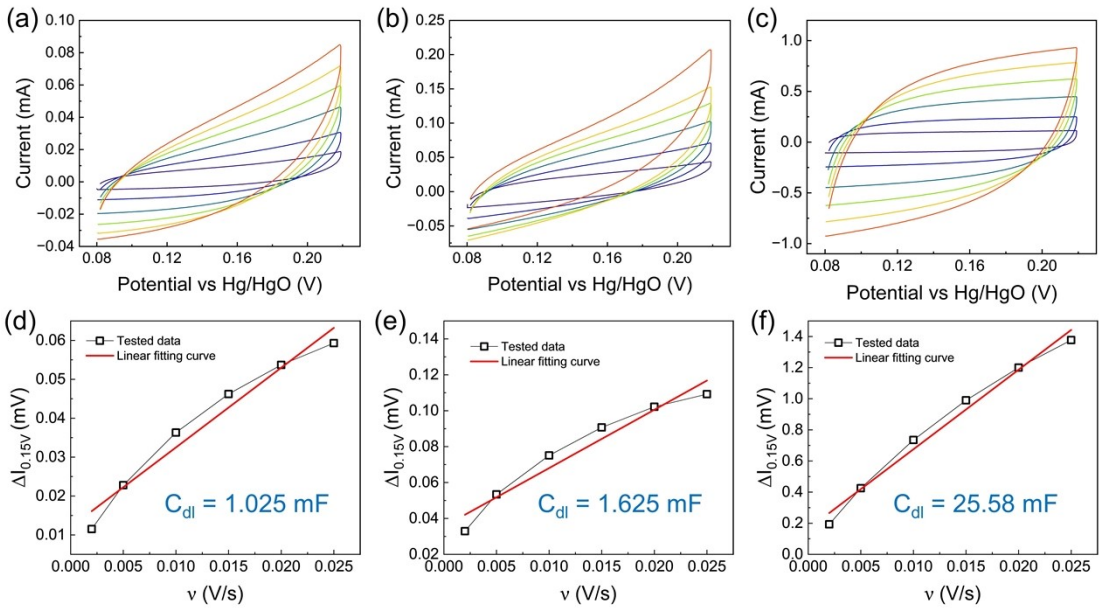

Figure S13. CVs taken in the non-faradic potential region under various scan rates for LW-CFF (a), LW-CFF-B (b) and LW-CFF-B-Ni (c). Corresponding plots of capacitive currents vs. scan rate values for LW-CFF (d), LW-CFF-B (e) and LW-CFF-B-Ni (f).

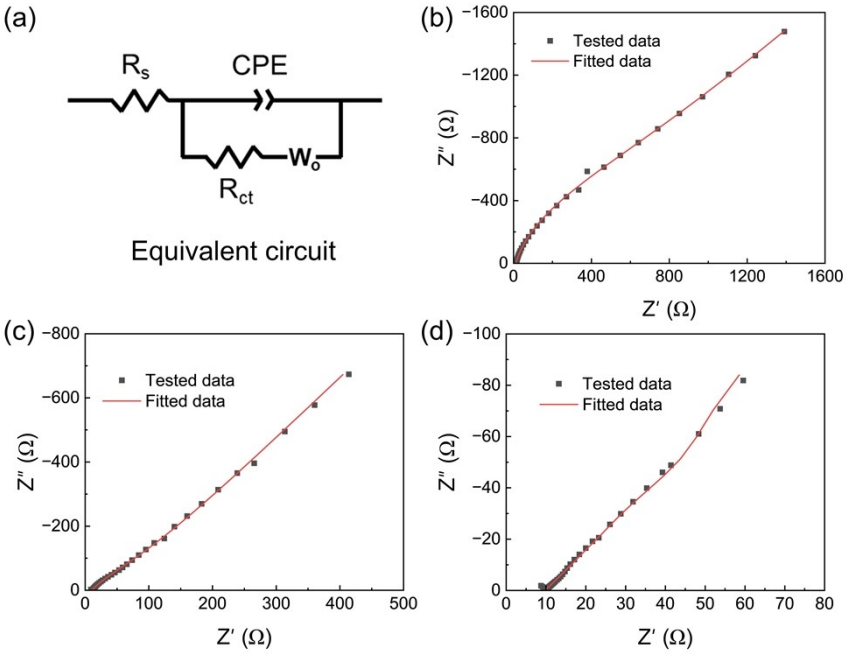

Figure S14. (a) Equivalent circuit used to simulated the electrode system. Nyquist graphs and fitted curves of tested electrochemical impedance spectroscopy (EIS) for LW-CFF (b), LW-CFF-B (c) and LW-CFF-B-Ni (d).

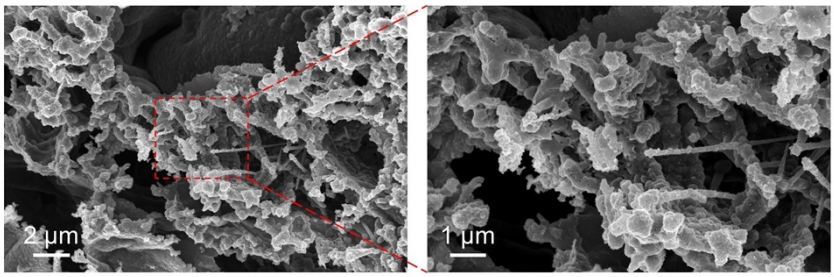

Figure S15. SEM images of LW-CFF-B-Ni after electrochemical testing ($Ni(NO_3)_2 \cdot 6H_2O$ concentration of 0.3 M).

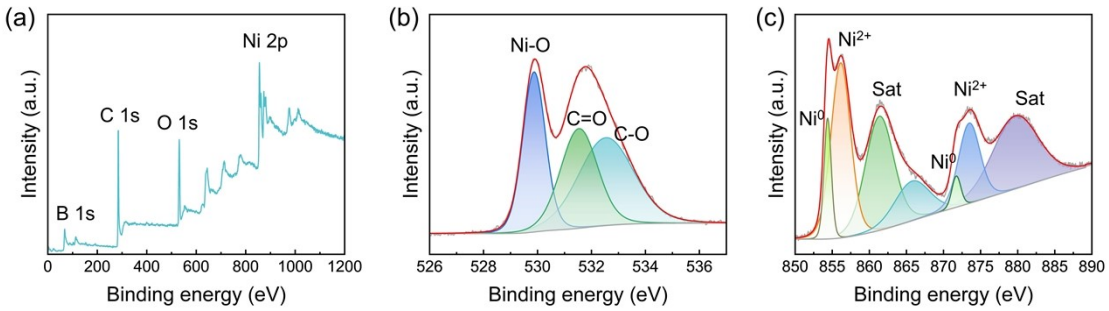

Figure S16. XPS survey spectrum (a), O 1s high-resolution deconvoluted spectra (b) and Ni 2p high-resolution deconvoluted spectra (c) of LW-CFF-B-Ni after electrochemical testing ($Ni(NO_3)_2 \cdot 6H_2O$ concentration of 0.3 M).

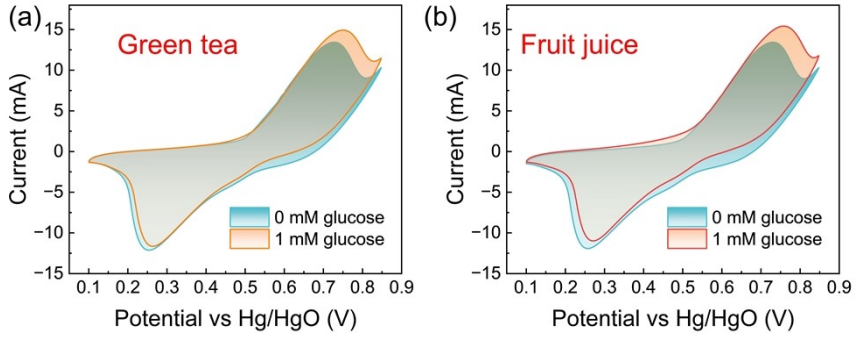

Figure S17. CV scans recorded without and with beverage sample addition (1 mM): (a) Green tea, (b) Fruit juice.

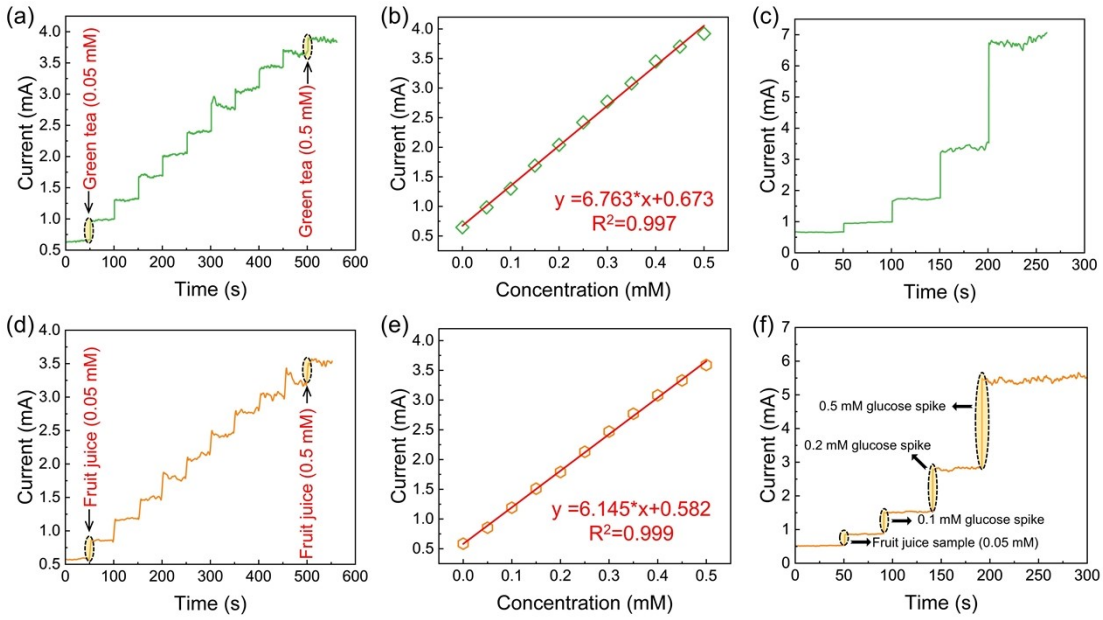

Figure S18. Amperometric response of LW-CFF-B-Ni sensor with a sequential injection of 0.05 mM beverage samples; Corresponding linear calibration curves for beverage samples; Amperometric response of LW-CFF-B-Ni for beverage samples taken before and after standard glucose spiking concentrations (applied potential: 0.6 V): (a)-(c) Green tea, (d)-(f) Fruit juice.

Table S1. Sheet resistance comparison of reported carbon skeleton materials.

Material	Sheet resistance (Ω/sq)	Reference
Paper-LIG	5.25	1
PI-LIG	8.5	2
rGO/Textile-LIG	87.6	3
Cork-LIG	32.8	4
Agglomerated cork-LIG	4.3	5
Natural Cork-LIG	10.8	6
Laser annealed CFR-PEEK	1.7	7
Paper-LIG	5	8
Kevlar textiles-LIG	2.86	9
PI-LIG	15	10
Carbon nanofiber (CNF) film	1.76	11
LW-CFF-B	1.23	This work

References

[1] X. Li, D. Su, Y. Gu, J. Zhang, S. Li, Y. Xiao, J. He, W. Wang, D. Li, *Applied Materials Today*, 2024, **36**, 102051.

[2] M. Chang, R. Tang, W. Zou, J. Xian, Z. Zhang, X. Liu, M. Qu, C. Zhang, *Adv. Mater. Interfaces*, 2024, **11**, 2301111.

[3] A. Lipovka, M. Fatkullin, S. Shchadenko, I. Petrov, A. Chernova, E. Plotnikov, V. Menzelintsev, S. Li, L. Qiu, C. Cheng, R. D. Rodriguez, E. Sheremet, *ACS Appl. Mater. Interfaces*, 2023, **15**, 38946-38955.

[4] M. Setti, E. Vaughan, R. Murray, L. Sygellou, A. J. Quinn, M. Riccò, D. Pontiroli, D. Iacopino, *Sens. Actuators, B*, 2025, **430**, 137352.

[5] T. Pinheiro, H. V. de Almeida, D. Nunes, R. Martins, E. Fortunato, *Mater. Horiz.*, 2025, **12**, 8194-8204.

[6] E. Vaughan, C. Santillo, M. Setti, C. Larrigy, A. J. Quinn, G. Gentile, M. Lavorgna, D. Iacopino, *Advanced Sensor Research*, 2023, **2**, 2300026.

[7] X. Hu, J. Huang, Y. Wei, H. Zhao, S. Lin, C. Hu, Z. Wang, Z. Zhao, X. Zang, *Adv Sci (Weinh)*, 2022, **9**, e2105499.

[8] T. Pinheiro, R. Correia, M. Morais, J. Coelho, E. Fortunato, M. G. F. Sales, A. C. Marques, R. Martins, *ACS Nano*, 2022, **16**, 20633-20646.

[9] D. Yang, H. K. Nam, T. D. Le, J. Yeo, Y. Lee, Y. R. Kim, S. W. Kim, H. J. Choi, H. C. Shim, S. Ryu, S. Kwon, Y. J. Kim, *ACS Nano*, 2023, **17**, 18893-18904.

[10] J. Lin, Z. Peng, Y. Liu, F. Ruiz-Zepeda, R. Ye, E. L. Samuel, M. J. Yacaman, B. I. Yakobson, J. M. Tour, *Nat. Commun.*, 2014, **5**, 5714.

[11] Y. Yao, K. K. Fu, S. Zhu, J. Dai, Y. Wang, G. Pastel, Y. Chen, T. Li, C. Wang, T. Li, L. Hu, *Nano Lett.*, 2016, **16**, 7282-7289.